European Journal of Endocrinology (2002) **147** 13–28 ISSN 0804-4643

REVIEW

Functional scintigraphy of the adrenal gland

Domenico Rubello[1,2], Chuong Bui[2], Dario Casara[1], Milton D Gross[3], Lorraine M Fig[3] and Brahm Shapiro[2]

[1]Nuclear Medicine Service, Department of Radiotherapy, Regional Hospital of Padova, Padova, Italy, [2]Division of Nuclear Medicine, Department of Radiology, University of Michigan Medical Center, Ann Arbor, Michigan, USA and [3]Nuclear Medicine Service, Ann Arbor Veterans Affairs Medical Center, Ann Arbor, Michigan, USA

(Correspondence should be addressed to D Rubello, Servizio di Medicina Nucleare 2^, Unità Operativa di Radioterapia, via Giustiniani 2, Azienda Ospedaliera di Padova, 35100 Padova, Italy)

Abstract

Over the last 30 years nuclear medicine imaging of the adrenal gland and its lesions has been achieved by the exploitation of a number of physiological characteristics of this organ. By seeking and utilising features which are quantitatively or qualitatively different from those of the adjacent tissues, functional depiction of the adrenal gland and its diseases, which in most cases retain the basic physiology of their tissue of origin, including both the cortex and the medulla, are now a useful clinical reality. Agents widely used in clinical practice include: (a) uptake and storage of radiolabelled cholesterol analogues via the low density lipoprotein (LDL) receptor and cholesterol ester storage pool in the adrenal cortex (^{131}I-6-β-iodomethyl-norcholesterol, ^{75}Se-selenomethyl-norcholesterol); (b) catecholamine type I, presynaptic, uptake mechanism and intracellular granule uptake and storage mechanism in the adrenal medulla and extra-adrenal paraganglia (^{131}I-, ^{123}I- and ^{124}I-meta-iodo-benzyl-guanidine (MIBG), ^{18}F-metafluoro-benzyl-guanidine); (c) cell surface receptor binding of peptides/neurotransmitters/modulators such as for the family of five subtypes of somatostatin receptors (^{123}I-tyr-octreotide, ^{111}In-DTPA-octreotide, ^{111}In-DOTA-octreotide and many others); (d) although not specific for the adrenal gland, increased glycolysis by tumours, particularly the most malignant varieties, ^{18}F-2-fluoro-D-deoxyglucose can thus be expected to depict certain malignant lesions such as malignant pheochromocytomas (particularly the minority which are not detected by MIBG) and adrenal incidentalomas (particularly when they occur in patients with known extra-adrenal malignancies).

There are a variety of adrenal tissue characteristics with potential for exploitation but which are not currently in clinical use, and which may, nevertheless, have potential as imaging agents. These include: (a) inhibitors of adrenal cortical steroid hormone synthesis enzymes (e.g. radiolabelled analogues of metyrapone); (b) radiolabelled lipoproteins which bind to adrenocortical LDL receptors; (c) inhibitors of catecholamine biosynthesis enzymes (e.g. radiolabelled analogues of tyrosine and related amino acids); (d) cell surface receptors for various peptides and hormones which may be over-expressed on adrenal cortical or adrenal medullary tumours (e.g. radiolabelled analogues of ACTH on adrenocortical cells of zona fasciculata or zona glomerulosa origin, neurotransmitter/hormone message peptides binding to cell surface receptors such as bombesin, vasoactive intestinal polypeptide, cholecystokinin and opiate peptides); (e) the adrenal cortex can also synthesise cholesterol *ab initio* from acetate, and preliminary studies with ^{11}C-acetate positron emission tomography have shown interesting results.

European Journal of Endocrinology **147** 13–28

Adrenal cortex

The adrenal cortex is constituted of three layers. The outer layer, the glomerulosa zone, produces mineralocorticoids (mainly aldosterone) under the control of the renin–angiotensin–aldosterone axis. Conversely, both the middle layer, the fasciculata zone, which produces glucocorticoids (mainly cortisol) and the inner layer, the reticulata zone, which produces sex hormones, are regulated by the hypothalamic–pituitary–adrenal axis.

Radiotracers for adrenal cortex imaging

Many radiotracers have been developed to image the adrenal cortex by exploiting different physiological mechanisms of steroid hormone uptake and metabolism. Many efforts have been made to label cholesterol, initially with ^{14}C-cholesterol (1) and then with ^{131}I (^{131}I-19-iodocholesterol; CL-19-I) (2, 3). ^{131}I-6-β-iodomethyl-norcholesterol (NCL-6-I) was initially recognised as a contaminant derived from the synthesis of CL-19-I and was shown to have at least a fivefold

greater avidity for adrenal cortex in rats and dogs and a greater *in vivo* stability than CL-19-I (4). Moreover, NCL-6-I showed a more rapid decrease of background activity in humans, making scintigraphic visualisation of the adrenal glands easier (3, 4). Another group of radiotracers comprises the inhibitors of adrenal cortical steroid hormone synthesis such as metyrapone and related compounds labelled with ^{123}I, ^{131}I, ^{111}In and ^{99m}Technetium (^{99m}Tc), but at present no successful clinical agent is available (5). Among the inhibitors of adrenal steroid synthesis there are also some positron-emission tracers such as ^{11}C-etiomidate and ^{11}C-metomidate that have been investigated (6). Another promising approach consists of labelling the low density lipoproteins (LDLs) with ^{111}In or ^{99m}Tc. LDLs are the principal carrier of cholesterol in the blood and for these there are specific receptors in the surface of the adrenocortical cells (7). Some other positron-emission tracers have been synthesised and among them ^{11}C-acetate was shown to accumulate in adrenal adenomas (8). Currently, NCL-6-I is the radiotracer most widely used in clinical practice for adrenal cortical imaging (9). A compound similar to NCL-6-I but labelled with ^{75}Se (^{75}Se-6-β-selenomethyl-norcholesterol; Scintadren, Nyocomed-Amersham) is available in Europe (10). The results obtained with Scintadren are comparable with those of NCL-6-I (10). The only marginal advantages of Scintadren over NCL-6-I is that the shelf life is up to 6 weeks and delayed imaging as late as 2 weeks can be obtained, when the background activity is negligible (10). NCL-6-I is carried in the circulation by LDL and is trapped into the adrenal cortex cells by specific LDL receptors (11). Once within the cytoplasm, NCL-6-I is esterified but does not appear to be further metabolised (11). However, there is an enterohepatic circulation which can cause an increase in the background colonic activity (12).

Patient preparation and NCL-6-I scintigraphic technique

It is an absolute requirement that drugs which may interfere with the hypothalamic–pituitary–adrenal axis (e.g. glucocorticoids) or on the renin–angiotensin–aldosterone axis (e.g. spironolactone, most diuretics, sympathetic inhibitors, oestrogens) be discontinued to avoid distortion of the biodistribution and misinterpretation of the scintigraphic imaging (11, 13). Moreover, attention should be paid to patients with high serum lipoprotein levels because decreased or even absent NCL-6-I uptake by the adrenal cortex has been observed, probably due to the expanded extra- and intracellular cholesterol pool and to the down-regulation of the specific adrenocortical LDL receptors (13). Saturated potassium iodine solution (SSKI) or Lugol's solution are given to the patient to block thyroidal uptake of free ^{131}I (14). Laxatives can be given to reduce the bowel background activity as well as a fatty meal or another cholecystagogue to reduce gallbladder activity (15). NCL-6-I is administered by slow intravenous injection at the dosage of 1 mCi/1.7 m^2 body surface area (13, 14). Baseline imaging (without hormonal manipulation) is usually obtained by planar scans of the abdomen 5 days after tracer administration; further imaging on days 6–7 (until day 14 with Scintadren) can be obtained, especially in cases with relatively high interfering bowel background activity (15). Single photon emission computed tomography (SPECT) acquisition has been suggested to be useful in some cases (16). In some pathologies, such as primary hyperaldosteronism and masculinising or feminising adrenal tumours, baseline NCL-6-I imaging has poor sensitivity due to the overlapping uptake of the adrenocorticotrophin (ACTH)-dependent normal adrenal tissue of the inner zones which can mask the uptake of a relatively small tumour (generally the size of Conn's tumour is less than 2 cm) (17). To improve the sensitivity of NCL-6-I scintigraphy in these patients, suppression of the normal adrenal cortex is achieved by pretreating the patient with dexamethasone. In normal subjects, during dexamethasone suppression (DS), the normal adrenal cortex is not visualised until day 5 post-injection when faint uptake can be seen due to a physiological breakthrough mechanism (17). Using DS NCL-6-I scintigraphy, imaging is usually obtained on days 3, 4 and 5 after tracer injection; longer delayed imaging (e.g. days 7 and 14) can be useful, especially when Scintadren is administered.

Normal NCL-6-I distribution

Following the injection, NCL-6-I concentration in the adrenal cortex is rapid, but to obtain an adrenal-to-background ratio favourable for imaging, the acquisition has to be delayed to days 4–5 (18). In normal subjects, faint NCL-6-I uptake is seen in the adrenals. The right adrenal is more cephalad and located deeper than the left adrenal and shows a slightly greater uptake as a common, physiologic finding; the left to right uptake ratio ranges from 0.9 to 1.2 (9, 11, 13, 14). Also, the overlapping liver uptake can contribute to the slightly greater uptake of the right adrenal. Uptakes differing by more than 50% exceed the normal asymmetry and should be considered abnormal (9, 11, 13, 14). The adrenal NCL-6-I uptake can be quantified by a region of interest (ROI) method and background and depth correction. The adrenal uptake in normal subjects ranges from 0.075 to 0.26% (mean 0.16%) of the administered dose (19). Gallbladder activity can interfere with the accurate visualisation of the right adrenal gland especially in DS scintigraphy. The lateral and anterior projections are useful to interpret the scan correctly (13, 14). Colonic activity can also be seen due to biliary excretion and subsequent enterohepatic circulation of NCL-6-I

(15). Activity in the thyroid and stomach can be observed in the presence of free ^{131}I.

Clinical applications of NCL-6-I scintigraphy

Cushing's syndrome

Bilateral symmetric visualisation. Bilateral symmetric visualisation is the typical finding of the ACTH-dependent corticoadrenal hyperplasia (11, 13, 14). This is the most frequent cause of Cushing's syndrome and can be due to a pituitary tumour or to ectopic ACTH production. Very high adrenal uptakes, exceeding 1% of the administered dose, strongly suggest the presence of an ectopic source of ACTH (14).

Asymmetric adrenal visualisation. Asymmetric adrenal visualisation, greater than 50%, suggests the presence of an ACTH-independent adrenocortical hyperplasia (11, 13, 14). It is worth noting that, in marked asymmetric nodular hyperplasia, computed tomography (CT) or magnetic resonance imaging (MRI) can underestimate the bilateral nature of the disease because it may reveal only a unilateral nodular involvement; this misdiagnosis can lead to inappropriate unilateral surgery (14, 17, 20). In contrast, NCL-6-I scintigraphy has been proven to accurately detect the asymmetric but bilateral nodular hyperplasia with high sensitivity (Fig. 1) (20).

Unilateral adrenal visualisation. Unilateral adrenal visualisation is the typical finding of the solitary adrenocortical adenoma (11, 13, 14). Because of the suppression of ACTH, the contralateral normal adrenal is not usually visualised (Fig. 2).

Bilateral non-visualisation. Once exogenous administration of glucocorticoids or the presence of high serum lipoprotein levels has been excluded, the bilateral non-visualisation pattern suggests the presence of an adrenocortical carcinoma (11, 13, 14, 21). Usually, the NCL-6-I concentration per gram of tissue is insufficient to allow the scintigraphic depiction of the malignant tumour. This, however, generally maintains the capability to secrete an excess of glucocorticoids which causes the suppression of ACTH and, consequently, the non-visualisation of the contralateral normal adrenal (21). In a small minority of patients, the adrenocortical carcinoma is depicted by NCL-6-I scintigraphy and in even fewer cases can its metastases also be visualised (21).

Adrenal remnant localisation. In Cushing's patients previously treated by bilateral adrenalectomy but who have persistent hypercortisolism, NCL-6-I scintigraphy has been proven to be a highly sensitive procedure for the detection of functioning remnants (11, 13, 14). Moreover, it should be emphasised that when an adrenal gland is destroyed or removed, the contralateral gland shows a compensatory hyperplasia (even nodular hyperplasia) and an increase in NCL-6-I uptake (22).

Primary hyperaldosteronism In patients with primary hyperaldosteronism, DS NCL-6-I scintigraphy is the procedure of choice in cases where CT scanning does not reveal an obvious Conn's adenoma, most frequently occurring in the presence of small bilateral hyperplasia. Early unilateral adrenal visualisation (<5 days) suggests the presence of a solitary adrenal adenoma (Fig. 3), whereas early bilateral visualisation (<5 days) suggests the presence of bilateral hyperplasia (Fig. 4) (11, 13, 14, 17, 23). However, the early images (before day 5) are not necessarily an absolute gold standard, especially using Scintadren which has a slower decrease in background activity in comparison with NCL-6-I; thus delayed imaging (until day 14) may be required. CT has been shown to be sensitive in detecting most adenomas but can fail in diagnosing

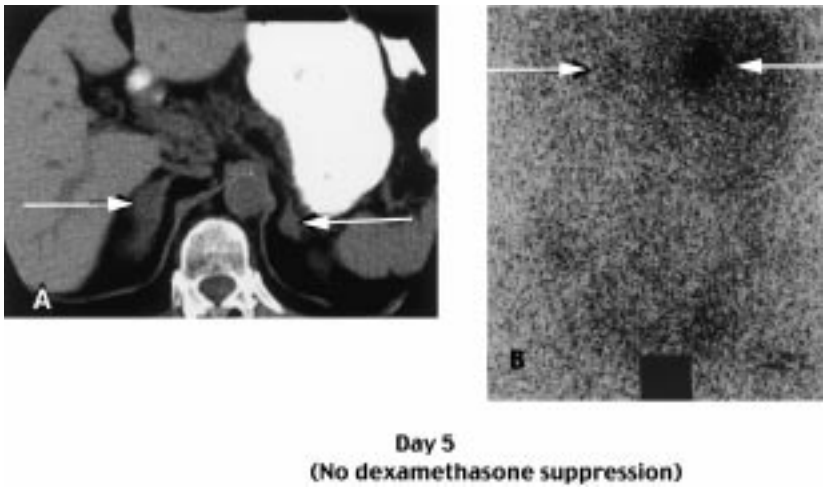

Figure 1 Bilateral, asymmetrical ACTH-dependent nodular hyperplasia causing Cushing's syndrome depicted by NCL-6-I. A 73-year-old female with biochemistry consistent with long-standing ACTH-dependent Cushing's syndrome who, at CT scan, showed a bilateral nodular enlargement of the adrenal glands, 4.6 cm on right, 1.3 cm on left. (A) Transverse CT abdomen showing bilateral asymmetrical adrenal enlargement, right larger than left, indicated by white arrows. (B) NCL-6-I posterior abdominal scan (without DS) with bilateral, asymmetrical tracer uptake, right adrenal much greater than left. Adrenal glands are indicated by white arrows.

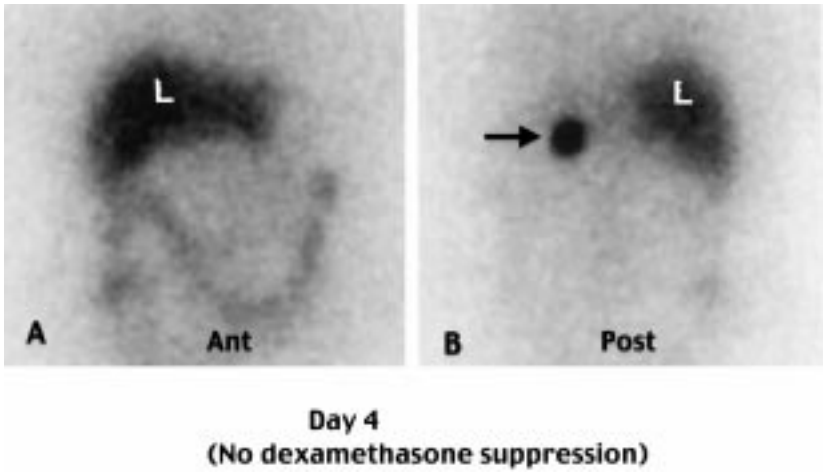

Figure 2 Adrenocortical adenoma causing Cushing's syndrome, depicted by NCL-6-I. A 48-year-old female with ACTH-independent Cushing's syndrome and a 3 cm left adrenal mass on CT scan which proved to be an adrenocortical adenoma when resected. (A) Anterior (Ant) and (B) posterior (Post) abdominal NCL-6-I scans without DS. The black arrow indicates left-sided, intense adrenal uptake. Note that the right adrenal is suppressed (not visualised) because of low ACTH; there is normal tracer uptake in the liver (L); faint colonic uptake is seen in the anterior view (A).

bilateral hyperplasia (11, 13). In contrast, NCL-6-I scintigraphy accurately depicts patients with bilateral hyperplasia (11, 13). It must be pointed out that early bilateral visualisation can also be observed in secondary hyperaldosteronism (24) and, thus, an accurate pre-scintigraphic differential diagnosis is of paramount importance. A late (> 5 days) adrenal visualisation is a typical finding in normal adrenals (17); however, this pattern can also be observed in some unusual cases of dexamethasone-suppressible hyperaldosteronism (24).

Adrenal hyperandrogenism and hyperoestrogenism These conditions are rare. The DS NCL-6-I scintigraphy may be useful in a manner similar to that for primary hyperaldosteronism and the interpretative criteria are the same (25).

Incidentalomas Due to the widespread use of high-resolution morphological imaging techniques such as CT, MRI and ultrasound, an exponentially growing number of unexpected adrenal masses, so-called incidentalomas, are being disclosed (26, 27). In most cases, these morphologic procedures are performed to investigate patients with abdominal pain or to stage an extra-adrenal neoplasm (28–30). The reported prevalence of incidentalomas in clinical series, including both cancer and non-cancer patients, ranges from 0.35 to 4.36% (26, 27) but in an autopsy series a fourfold greater prevalence was found (31). The discovery of an adrenal incidentaloma represents a serious diagnostic and therapeutic dilemma in clinical practice (e.g. benign versus malignant lesion; prompt surgical removal versus 'wait and see' policy). It has been clearly documented that the majority of incidentalomas are benign masses that do not require an aggressive approach (29). However, if a solitary metastatic lesion is present without evidence of other metastatic spread, the patient could benefit from the surgical extirpation of such a lesion. In a large meta-analysis on adrenal incidentalomas performed by Kloos *et al.* (27), the prevalence of adrenal cortex adenoma was estimated to be 36–94% in non-oncologic patients and 7–68% in oncologic patients, while adrenal metastases were found in 0–21% of the non-oncologic patients and in 32–73% of the oncologic patients. Moreover, cysts were found in 4–22% of cases, myelolipoma in 7–15%, pheochromocytoma in

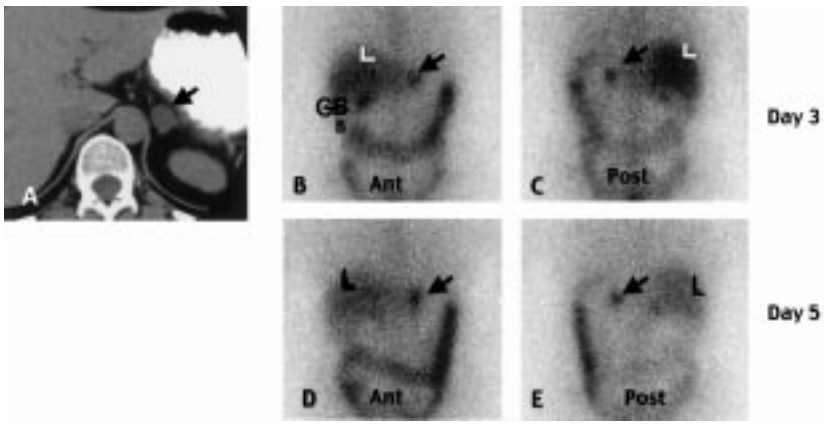

Figure 3 Left adrenal aldosteronoma demonstrated with NCL-6-I under DS. A 57-year-old female with biochemical evidence of hyperaldosteronism and a 2 cm left adrenal mass on CT scan. (A) Transverse abdominal CT scan demonstrating 2 cm left adrenal mass (black arrow). (B and C) Anterior (Ant) and posterior (Post) abdominal NCL-6-I scans on day 3 post-injection. (D and E) Anterior and posterior abdominal NCL-6-I scans on day 5 post-injection. Left-sided abnormally increased adrenal tracer uptake is indicated by black arrows. Note that adrenal imaging occurs early, before day 5 (B and C). There is normal uptake in liver (L), bowel (B) and gallbladder (GB). Note also that great care should be taken not to confuse GB with the right adrenal gland (B).

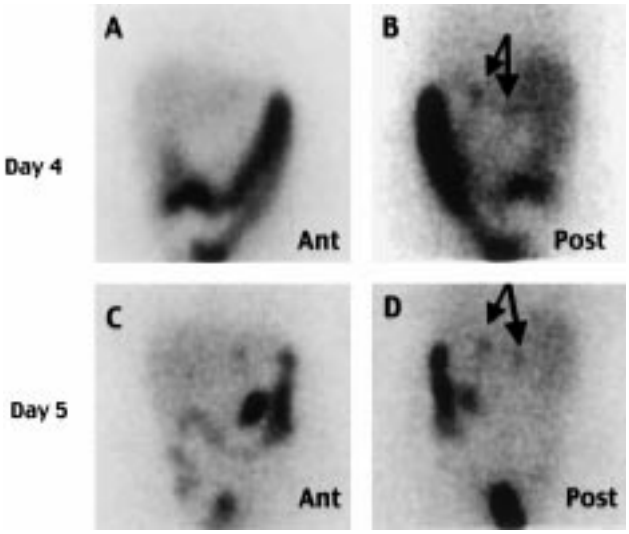

Figure 4 Bilateral adrenal hyperplasia causing primary hyperaldosteronism demonstrated by NCL-6-I under DS. A 35-year-old female with hypertension, biochemical evidence for hyperaldosteronism and a report of bilateral adrenal thickening on CT scan performed elsewhere. (A and B) Anterior (Ant) and posterior (Post) abdominal NCL-6-I scans on day 4 post-injection. (C and D) Anterior and posterior abdominal NCL-6-I scans on day 5 post-injection. Bilateral abnormally premature adrenal visualisation on day 4 is indicated by black arrows in (B), and again at day 5 in (D). Note the faint normal liver uptake and intense, extensive activity in the large bowel, this may be especially intense in primary hyperaldosteronism due to hypokalaemia reducing colonic motility.

0–11%, and other adrenal lesions with smaller percentages. Interestingly, the prevalence of pseudo-adrenal masses, e.g. lesions arising from organs located near to the adrenals such as the stomach, pancreas and kidneys is by no means negligible, accounting for 0–10% of all incidentalomas (27). The diagnostic algorithm to be adopted in patients with incidentalomas is an object of debate in the literature. However, once those lesions with an obvious radiological diagnosis (e.g. simple cyst, myelolipoma) are excluded, a rational diagnostic approach to incidentalomas should comprise the following steps: (a) obtain an accurate clinical and biochemical profile to identify those patients who present with a hypersecretory mass; these masses usually require surgical removal, and (b) in non-hypersecretory masses, which represent the majority of cases, it is required that a differential diagnosis of benign versus malignant be made, bearing in mind that the probability of malignancy is rather low (27, 29). CT and MRI are widely used for this purpose but none of the parameters investigated with both these procedures has been proven to be sensitive and specific enough (32). A size criterion of, typically, 5 cm has been empirically established to select those patients who are candidates for surgery (33). There is some evidence in the literature that the relative risk of malignancy increases with the increasing of the size of the mass (34). However, the published data are controversial. In several series, the prevalence of benignity has been reported as high as 76–100% in large masses greater than 5 cm (35, 36). Conversely, malignant tumours have been documented in relatively small adrenal masses, sized less than 2.5 cm (33, 37). Serial CT imaging has been used, in that those masses showing a progressive growth are more likely to be malignant (28, 30). However, those patients with malignant masses diagnosed only after demonstrable growth on serial CT studies may suffer from a delay in the diagnosis and appropriate therapy (27). One of the most useful CT criteria is the unenhanced CT attenuation coefficient (38). An attenuation coefficient of 0 or less Hounsfield Units (HU) was found to be 100% specific in distinguishing benign adenomas from metastases (27, 38); however, a rather low sensitivity was reported, ranging from 33 to 47% (27, 39). Increasing the threshold of the HU attenuation coefficient, a better sensitivity was achieved but with a concomitant loss in specificity (39). Among the MRI criteria, the chemical shift technique, based on the difference of resonance frequency between protons in water and lipids, has shown promising results. The loss of signal intensity using the opposed-phase imaging technique is a typical finding of lipid-rich masses such as benign cortical adenomas (40). However, some lipid-depleted cortical adenomas as well as occasional cases of lipid-rich metastases and pheochromocytomas have been described (41, 42). Fine needle aspiration (FNA) biopsy has been proven to be highly accurate (80–100%) in distinguishing benign adrenal masses from metastatic disease (30, 43). However, the distinction of benign cortical adenomas from well-differentiated adrenocortical carcinomas is often difficult (43). Moreover, in patients with pheochromocytomas, FNA biopsy can cause a severe, even fatal, hypertensive crisis (27). Adrenocortical radiocholesterol scintigraphy has been proven to be the most accurate non-invasive imaging technique in differentiating benign cortical adenoma from space-occupying or destructive adrenal lesions (26, 27, 44). Three scintigraphic patterns can be observed in patients with incidentaloma: (a) the *concordant pattern* reveals increased tracer uptake in the adrenal mass depicted at morphologic imaging; this pattern is consistent with the presence of a benign cortical adenoma or nodular hyperplasia (Fig. 5); (b) the *discordant pattern* reveals an absent, decreased or distorted uptake by the adrenal mass depicted at morphologic imaging; this pattern is consistent with the presence of a space-occupying or destructive lesion (e.g. metastasis, adrenocortical carcinoma, adrenomedullary tumour, haemorrhage, cyst, granulomatous disease) (Figs. 6 and 7) ; (c) the *non-lateralising pattern* reveals normal symmetrical adrenal uptake. In masses greater than 2 cm the *non-lateralising pattern* is consistent with the presence of a pseudoadrenal mass, while in masses smaller than 2 cm, due to

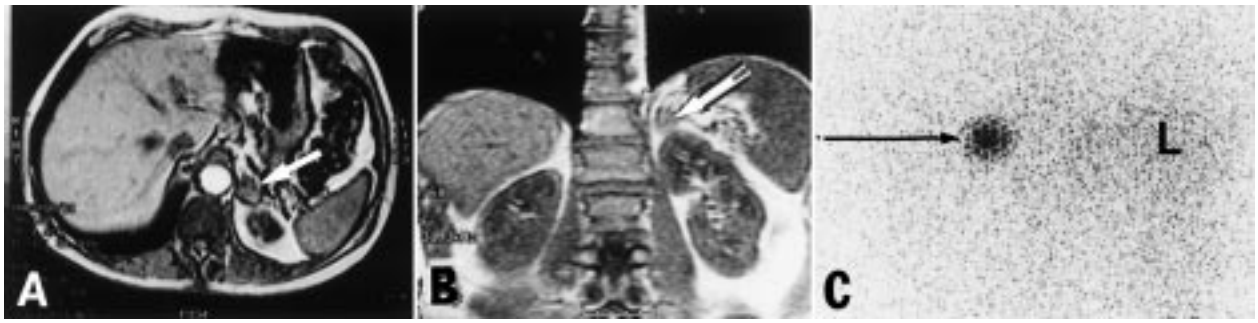

Figure 5 Left-sided incidentally discovered adrenal mass showing a concordant pattern. The patient underwent an abdominal CT scan for investigation of abdominal pain and at low attenuation a left adrenal mass was discovered. Screening biochemical tests of adrenocortical and adrenomedullary hormones were all within the normal range. The adrenal mass was subsequently studied by MRI and NCL-6-I scintigraphy. (A) Transverse abdominal CT scan. Left adrenal mass indicated by the white arrow. (B) Coronal MRI image of the lower thorax and upper abdomen. Left adrenal mass indicated by the white arrow. (C) Posterior abdominal NCL-6-I scan revealing an intense tracer uptake in the left adrenal (black arrow). Note the faint normal liver uptake (L). All the above findings together indicate that the left adrenal mass is a benign, non-hypersecretory adenoma. Note the contralateral adrenal gland shows no uptake due to suppression by the adenoma even though all parameters of cortisol secretion were within the normal wide range.

the limitations of the spatial resolution of scintigraphy, this pattern is non-specific (27).

A *concordant pattern* has 100% accuracy in predicting the presence of a benign adrenal mass, and a *discordant pattern* or a *non-lateralising pattern* in masses greater than 2 cm have 100% accuracy in predicting the absence of a non-hypersecretory adrenal adenoma and, thus, leads to suspicion of malignancy (27). Perhaps ^{18}F-2-fluoro-D-deoxyglucose (^{18}F-FDG) positron emission tomography (PET) might play a role in further investigation of the possibility of malignancy in incidentalomas with a discordant pattern or in those with a non-lateralising pattern in masses smaller than 2 cm. This topic is discussed below.

Sympathomedulla

The adrenal medulla represents the largest component of the sympathetic nervous system that also comprises the nervous ganglia that are widely and variably distributed through the body from the base of the skull to the floor of the pelvis (45). Epinephrine, norepinephrine and dopamine are the most frequently produced catecholamines: they are synthesised from tyrosine and then stored within intracytoplasmic granules linked to chromogranin and other proteins. Catecholamines can serve as hormones that are released into the circulation (e.g. adrenal medulla) or neurotransmitters that are secreted into the synaptic cleft. A substantial fraction of the secreted catecholamines re-enters sympathomedullary cells by two re-uptake mechanisms: the type I re-uptake mechanism is energy, sodium and temperature dependent, saturable and specific, while type II re-uptake mechanism is based on passive diffusion and is relatively non-specific. Once it re-enters the cytoplasm, catecholamines are once again concentrated in the storage granules.

Tumours can arise both from the adrenal medulla and sympathetic nervous ganglia (45, 46). The most

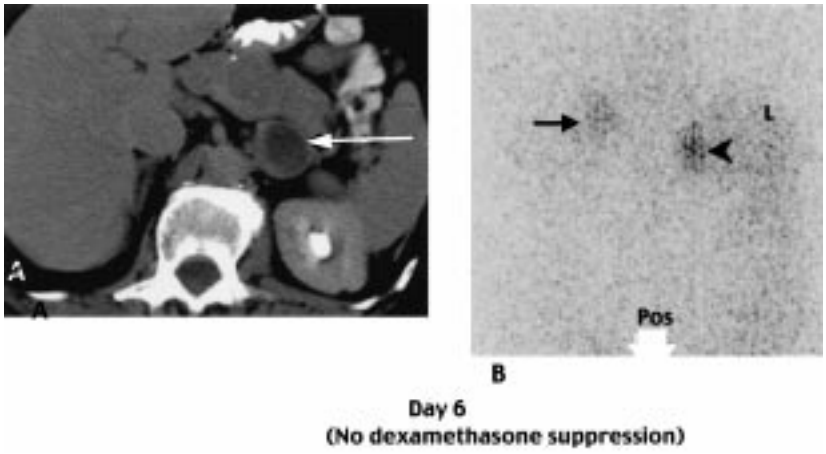

Figure 6 Left-sided incidentally discovered adrenal mass showing a discordant pattern. A 61-year-old male 5 years post-cistectomy and neo-bladder construction. Serial staging and surveillance CT scans showed an enlarging left adrenal mass. Screening hormonal measurements showed no hypersecretion. Laparoscopic adrenalectomy revealed a pheochromocytoma. (A) Detail of a tranverse CT of the abdomen showing left adrenal mass (white arrow). (B) NCL-6-I posterior (Pos) abdominal scan showing faint normal liver tracer uptake (L), normal right adrenal tracer uptake (arrow head) and faint and splayed out left adrenal tracer uptake (discordant pattern) (black arrow).

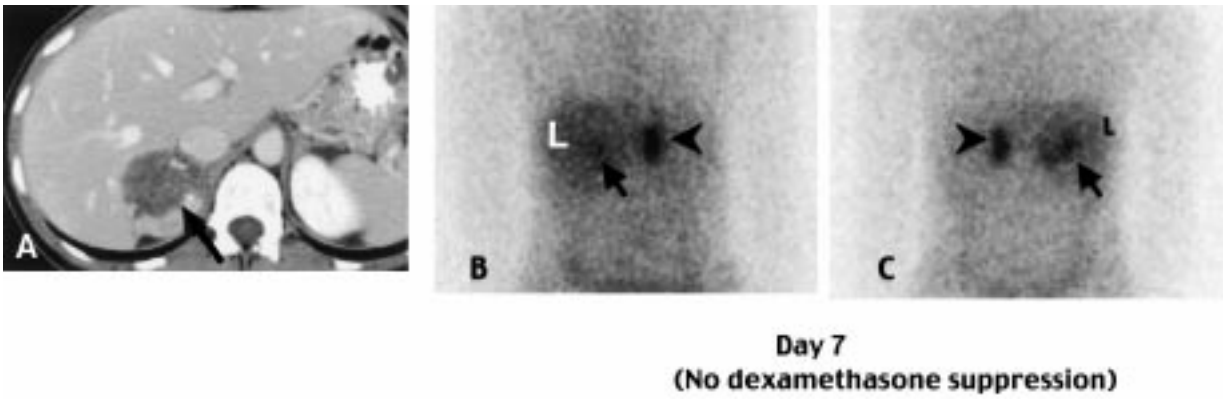

Figure 7 Low grade right adrenocortical carcinoma showing faint NCL-6-I visualisation. A 41-year-old female with incidental discovery of a 5 cm right adrenal mass which was stable on serial CT imaging. Biochemical investigations revealed no evidence for any hormonal hypersecretion. At surgical excision, the tumour was encapsulated and there was no evidence of local extension or vascular invasion. (A) Tranverse abdominal CT scan. The black arrow indicates a 5 cm right adrenal mass. (B and C) Anterior and posterior abdominal NCL-6-I scans, without DS. The black arrows indicate faint, patchy, irregular uptake in right-sided corticoadrenal carcinoma. L = normal liver uptake. The arrow heads indicate normal adrenocortical tracer uptake in the left adrenal gland. Note that at variance with the case described here, the vast majority of adrenocortical carcinomas are not depicted by NCL-6-I and in the case of adrenal cancer hypersecreting cortisol, uptake in the contralateral normal adrenal gland is suppressed.

frequent type of tumour is the pheochromocytoma which generally arises from the adrenal medulla and in most cases is a solitary, benign lesion. However, in about 10% of cases, pheochromocytomas arise from nervous ganglia, so-called paraganglioma. Paragangliomas are more likely to be multicentric and/or malignant than pheochromocytomas and these conditions occur in about 10% of cases (46). Bilateral pheochromocytomas or hyperplasia are usually observed in patients with multiple endocrine neoplasia (MEN) both type IIA and type IIB, and in patients with von Hippel–Lindau or von Recklinghausen syndrome (46).

Radiotracers specific for sympathomedullary imaging

Many radiotracers have been developed for the localisation in tumours arising from the adrenal medulla and nervous ganglia, such as radiolabelled catecholamines (^{14}C-dopamine, ^{11}C-epinephrine), radiolabelled enzyme inhibitors of catecholamine biosynthesis (various tyrosine derivates) and neuronal blocking agents (bretylium, guanethidine analogues) (47). Among guanethidine analogues, meta-iodo-benzyl-guanidine (MIBG) labelled with various iodine isotopes has been proven to be the most reliable tracer for human studies (48). The MIBG molecular structure is similar to that of norepinephrine: it is trapped by the sympathetic cells by means of the type I re-uptake mechanism and is then concentrated within the storage granules, but it does not undergo further metabolism (49). Recently, some positron-emitting tracers such as ^{11}C-hydroxyephedrine, ^{11}C-epinephrine, ^{18}F-metafluoro-benzyl-guanidine and ^{124}I-MIBG have been investigated with promising results (47). At the moment, the most widely used tracer in clinical practice is MIBG labelled with ^{131}I or ^{123}I.

Patient preparation and MIBG scintigraphic technique

Some drugs are known or may be expected to interfere with type I re-uptake and/or intracytoplasmic granular storage, mainly labetalol (which in addition to α- and β-adrenergic blocking has tricyclic properties), reserpine, sympathomimetics, calcium antagonists, tricyclic antidepressants and cocaine (47–51). Patients should be taken off these drugs for an appropriate time prior to scintigraphy. To control hypertension, α-blockers (such as phenoxybenzamine) or β-blockers (such as propranolol) can be administered (50). To minimise free radioiodine thyroidal uptake, pretreatment with SSKI or Lugol's solution is given (47–49). Laxatives can be given to decrease gastrointestinal activity. ^{131}I-MIBG at a dosage of 0.5-1.0 mCi or ^{123}I-MIBG at a dosage of 2-10 mCi are administered by slow intravenous injection (47–50). Imaging is obtained at 24, 48 and 72 h with ^{131}I-MIBG (some authors suggest additional imaging on day 7 (52)), and at 4–6 and 24 h and sometimes 48 h with ^{123}I-MIBG. Whole body scans and spot planar images are obtained. Using ^{123}I, SPECT imaging can also be acquired (53). In patients with malignant disease that are candidates for radioisotope therapy, ^{131}I-MIBG is used for dosimetric purposes (47).

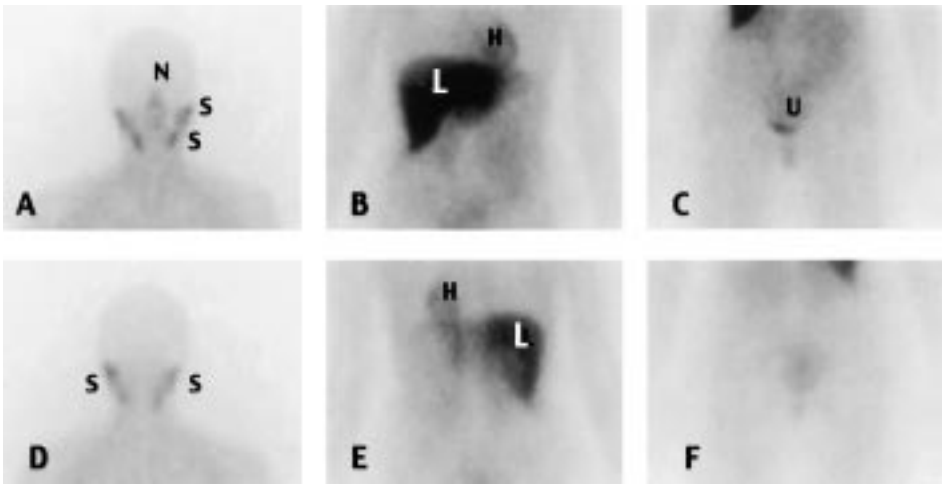

Figure 8 Normal, physiological ^{123}I-MIBG biodistribution. (A) Anterior head, neck and upper chest. (B) Anterior chest and abdomen. (C) Anterior lower abdomen and pelvis. (D) Posterior head, neck and upper chest. (E) Posterior chest and abdomen. (F) Posterior lower abdomen and pelvis. N = nasopharynx, S = salivary glands, L = liver, H = heart, U = urinary bladder.

Normal MIBG biodistribution

In normal subjects, salivary glands, liver, spleen and bladder are commonly depicted. Kidney uptake is early and may be transient. A variable degree of uptake in the myocardium and lungs can be observed. Thyroid and stomach can be visualised if free radioiodine is present and, in delayed images, colonic activity can also be seen (Fig. 8) (54). Normal adrenals are uncommonly and faintly visualised with ^{131}I-MIBG (< 20% of cases at 48 h) (54) whereas a faint uptake is frequently seen using ^{123}I-MIBG (Fig. 9) (47). In contrast, most adrenal pheochromocytomas show intense focal uptake (Figs 10 and 11). The MIBG uptake by the adrenomedulla can be calculated using an ROI method with background and depth correction (55–57): in normal subjects it ranges from 0.01% to 0.22% of the injected dose 22 h post-injection (55). Interestingly, Bomanji *et al.* (56, 57) observed that in the presence of pheochromocytoma, paraganglioma or neuroblastoma with elevated plasma and urinary catecholamines, the unaffected adrenal medullary tissue retains the capacity of trapping MIBG with uptake values similar to normal subjects (56). Moreover, a positive correlation was found between MIBG uptake and the number of storage granules in the tumoural tissue, but not with plasma or urinary catecholamines, suggesting that the uptake and storage of MIBG by the normal adrenal tissue is not regulated by a catecholamine feedback mechanism (57).

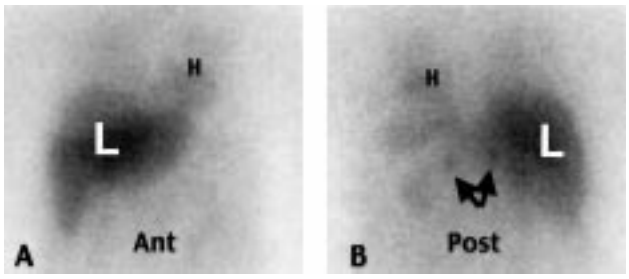

Figure 9 Normal, physiological adrenal medullary ^{123}I-MIBG uptake. (A) Anterior (Ant) lower chest and abdomen and (B) posterior (Post) lower chest and abdomen. H = heart, L = liver. Black arrows indicate bilateral physiological adrenal medulla uptake.

Principal clinical applications of MIBG scintigraphy

MIBG has been proven to be highly accurate in locating tumours arising from sympathomimetic nervous system cells. Evaluating a group of 600 patients with pheochromocytoma, Shapiro & Gross (58) found an 88% sensitivity and a 99% specificity. Slightly greater sensitivity has been reported with ^{123}I-MIBG and SPECT imaging than with ^{131}I-MIBG (53). It should be emphasised that MIBG scintigraphy is particularly useful for the identification of multicentric or metastatic pheochromocytomas due to the ability to evaluate the entire body (59) (Fig. 12). It may be difficult to distinguish benign multicentric from multiple metastatic pheochromocytomas unless metastatic foci are depicted in areas other than those in which sympathetic tissue is normally found (e.g. bone, bone marrow, lymph nodes, liver) (53, 59). In patients with neurofibromatosis, MIBG has been reported to be useful in the differential diagnosis of pheochromocytoma from retroperitoneal neurofibromata (60). The accuracy of MIBG is also very high in patients with neuroblastoma, with reported sensitivity of 90% and specificity of 99% (61). Both in malignant pheochromocytoma and neuroblastoma, MIBG has been proven to be of use

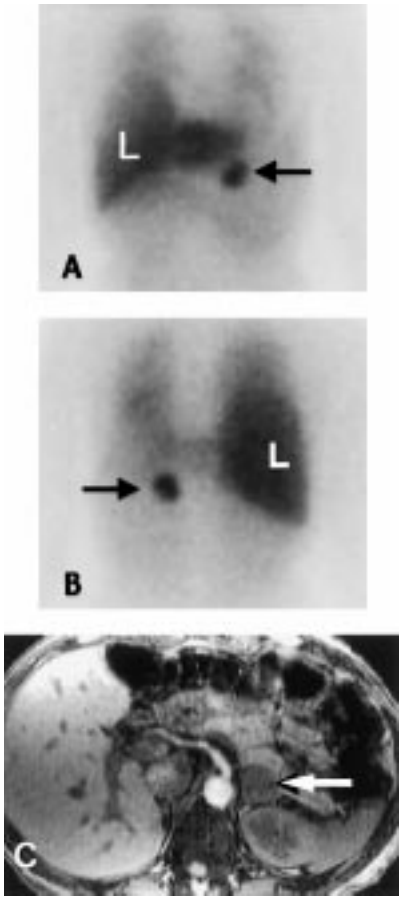

Figure 10 Left adrenal pheochromocytoma demonstrated by ^{123}I-MIBG and MRI. A 50-year-old female with hypertension, a history of neurofibromatosis, elevated plasma catecholamines and a 3 cm left adrenal mass on MRI. (A) Anterior abdomen scan. L = normal liver uptake. The black arrow indicates intense, abnormal focal tracer uptake in the region of the left adrenal gland. (B) Posterior abdomen scan. L = liver. The black arrow indicates left adrenal pheochromocytoma. (C) Abdominal MRI, transverse section with left adrenal pheochromocytoma indicated by the white arrow.

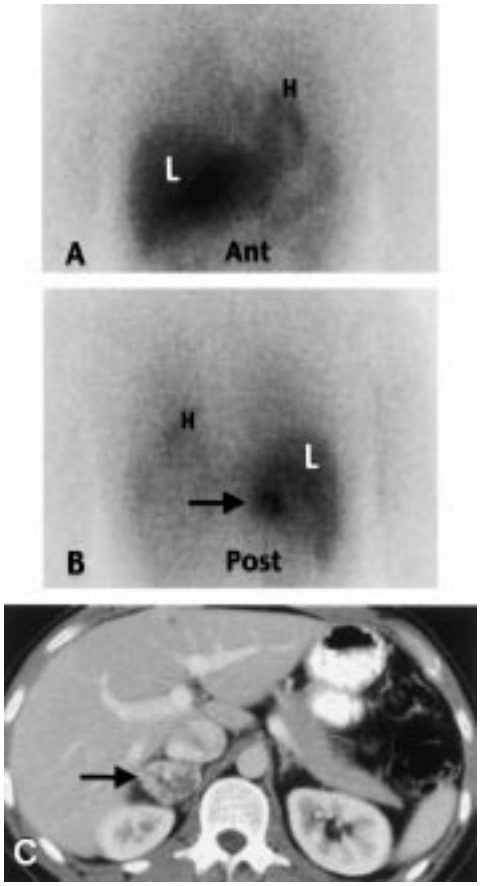

Figure 11 Right adrenal pheochromocytoma demonstrated by ^{123}I-MIBG and CT scans. A 31-year-old male with a family history of von Hippel–Lindau disease and demonstrated to carry the gene, having intermittent palpitations, and undergoing systematic screening. (A and B) Anterior (Ant) and posterior (Post) chest and abdomen scans. L = liver, H = heart. The black arrow in (B) indicates abnormal focus of ^{123}I-MIBG uptake in the region of the right adrenal gland. (C) Transverse abdominal CT sections. The black arrow indicates right adrenal pheochromocytoma lying between the inferior vena cava and the right kidney.

not only in the staging of the disease but also during follow-up to distinguish scar from persistent or recurrent disease, to permit early diagnosis of relapses, to monitor the response to treatment, and to select those patients who are candidates for treatment with ^{131}I-MIBG (58).

Other clinical applications of MIBG scintigraphy

There are a number of series on the use of MIBG scintigraphy in other neuroendocrine tumours, especially medullary thyroid carcinoma (MTC) and carcinoid (50, 61). With regard to MTC, there are two different indications for MIBG scintigraphy. The first hinges on the fact that familial MTC is often associated with a MEN syndrome and that, both in the IIA and IIB forms, pheochromocytoma or adrenal medulla hyperplasia can be present together with the MTC (62). In these patients, MIBG scintigraphy is of great use for the early detection of pheochromocytoma, even in the absence of a clinically evident hypersecretory syndrome. In this condition, given our inability to non-invasively determine the presence of malignancy and to predict the risk of spontaneous hypertensive crisis that can be severe and even fatal, a surgical curative approach is advisable (27). The second indication concerns the use of MIBG scintigraphy in the post-surgical follow-up of MTC patients with increased calcitonin and/or carcino-embryonic antigen (CEA) levels to visualise metastatic foci of MTC; unfortunately, a rather low sensitivity, ranging from 33 to 45% has been reported in these patients, particularly for detection of liver tumour deposits (61). For the same clinical purpose, other radiotracers such as ^{201}thallium chloride,

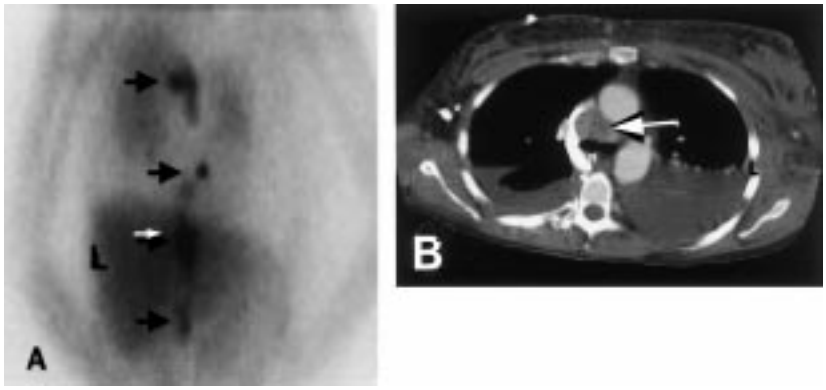

Figure 12 Malignant metastatic pheochromocytoma demonstrated by ^{123}I-MIBG and CT scans. A 31-year-old female after bilateral adrenalectomy with hypertension, end-stage renal failure and recent superior vena cava (SVC) obstruction. (A) Anterior chest and abdomen scan. L = normal liver uptake. Arrows indicate multiple abnormal foci of ^{123}I-MIBG uptake depicting multiple metastatic pheochromocytoma deposits in superior mediastinum, lower posterior mediastinum and para-aortic region. (B) Thoracic transverse CT section. The white arrow indicates the superior mediastinal mass responsible for SVC obstruction.

^{99m}Tc-(V)-DMSA (olimercaptosuccinic acid), anti-CEA monoclonal antibodies, ^{99m}Tc-methoxy-isobutyl-isonitrile and ^{111}In-octreotide have shown sensitivity rates superior to MIBG, ranging from 65 to 85% (50, 61, 63, 64). As with MTC, the sensitivity of MIBG scintigraphy in carcinoid patients is less than ideal, with reported values ranging from 30 to 60% (50, 61).

Other radiotracers for symphatomedullary imaging

Somatostatin analogues Somatostatin analogues, such as ^{123}I-tyr3-octreotide, ^{111}In-DTPA-octreotide (^{111}In-octreotide; where DTPA is diethylene-triamine-penta-acetate) and ^{111}In-DOTA-octreotide (where DOTA is tetra-aza-cyclododecane-N,N′N″,N‴-tetra-acetate), have been extensively investigated for imaging of sympathomedullary and other neuroendocrine tumours, as well as of other non-tumoural diseases in which an over-expression of somatostatin receptors is present on the cell surface (65). ^{111}In-octreotide is currently widely utilised in clinical practice. Octreotide is an 8 amino acid peptide that binds specifically to the family of somatostatin receptors, with greater affinity for subtypes II and V (66). Some promising β-emitting radiotracers such as ^{86}Y-DOTA-tyr3-octreotide have been synthesised for PET imaging and are under investigation (65).

Patient preparation and ^{111}In-octreotide scintigraphic techniques ^{111}In-octreotide scintigraphy does not require specific patient preparation. The discontinuation of somatostatin analogues 1 week prior to scintigraphy is generally recommended (50). Imaging is usually obtained 4–6 and 24 h after the intravenous injection of 3–6 mCi ^{111}In-octreotide. Whole body, spot planar and SPECT images should be obtained. SPECT has higher sensitivity than planar imaging in some series (67). Laxatives can be given to reduce activity in the bowel.

Normal ^{111}In-octreotide biodistribution In normal subjects, relatively high uptake is observed in the spleen, liver, kidneys and bladder. Faint uptake can also be observed in the pituitary, thyroid and salivary glands. Bowel activity is usually seen and generally increases in delayed images (66). Cardiovascular blood-pool activity is commonly seen in the early images and, thus, delayed images are more useful to depict mediastinal lesions.

Clinical applications of ^{111}In-octreotide scintigraphy ^{111}In-octreotide scintigraphy has demonstrated high sensitivity for detection of pheocromocytoma (86%), paraganglioma (100%) and neuroblastoma (89%) (66). However, an adrenal mass can be obscured by the presence of an intense kidney activity. Moreover, ^{111}In-octreotide is not a specific tracer for symphatomedullary tumours as it also shows significant uptake in most other neuroendocrine tumours, both benign and malignant, as well as in some non-endocrine tumours (e.g. breast cancer, Hodgkin's disease and non-Hodgkin's lymphoma, meningioma, etc) and also in several non-tumoural granulomatous diseases (e.g. sarcoidosis, tuberculosis, etc) and auto-immune disorders (e.g. Graves' disease, rheumatoid arthritis, etc) (50). This uptake is related to the widespread distribution throughout the body of cells expressing somatostatin receptors on their surface, including activated lymphocytes (50). Thus, it seems reasonable to consider ^{111}In-octreotide scintigraphy as a second-choice technique for sympathomedullary imaging after MIBG scintigraphy, especially when the MIBG is completely or partly false negative (Fig. 13). Conversely, due to its high sensitivity, ^{111}In-octreotide scintigraphy can be considered as the scintigraphic imaging technique of first choice in neuroendocrine tumours such as carcinoids (50, 67), pituitary tumours (68) and pancreatic and gastro-intestinal amine precursor uptake and decarboxylation (APUD)-omas (50, 69, 70). With particular regard to carcinoids, in an extensive meta-analysis, Hoefnagel (50) calculated an 86% sensitivity in a group of 451 patients evaluated with ^{111}In-octreotide, while in a group of 275 patients evaluated with ^{131}I-MIBG a sensitivity of 70% was found. Furthermore, in MTC patients, ^{111}In-octreotide scintigraphy has revealed a

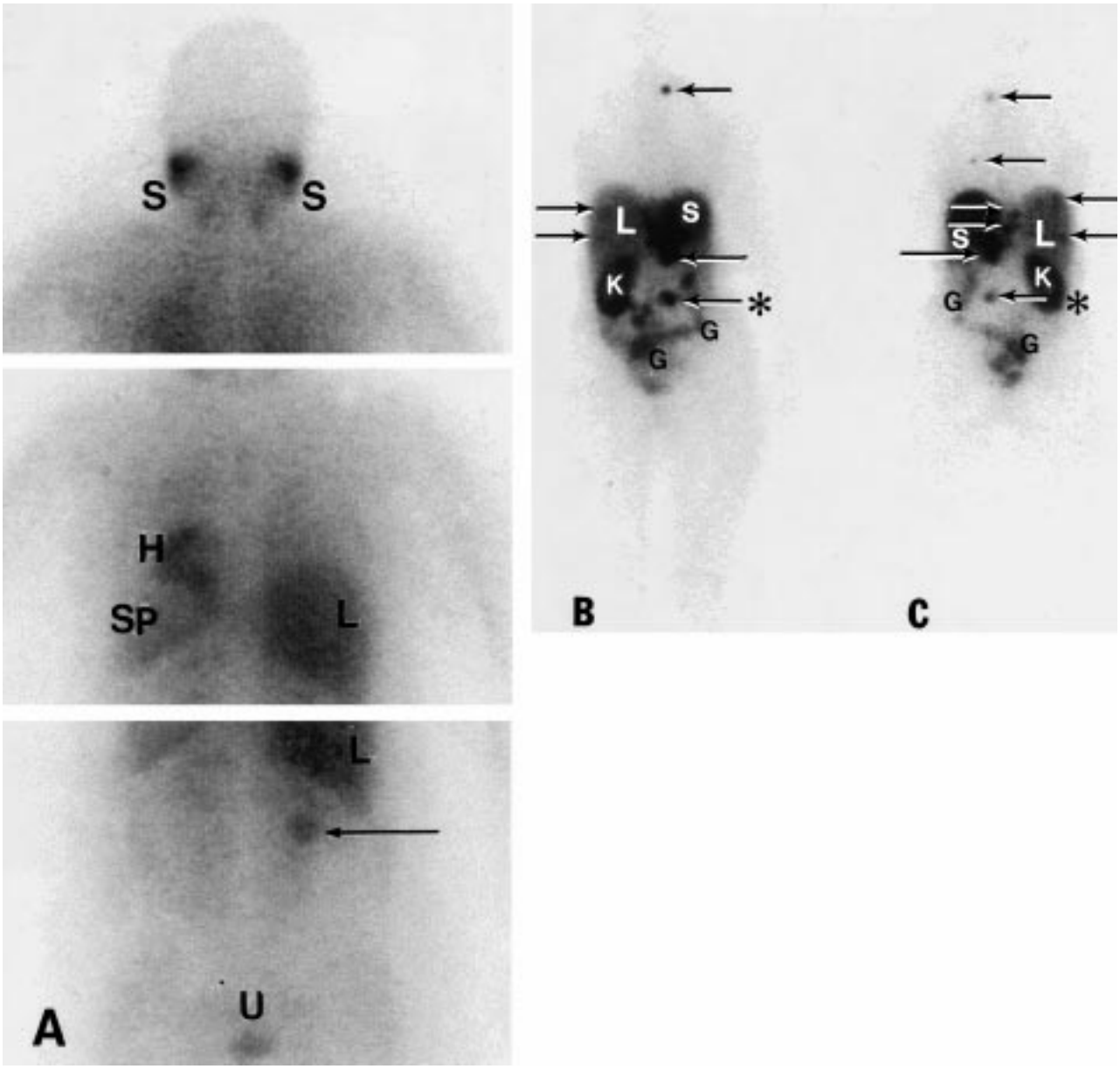

Figure 13 Widespread metastatic pheochromocytoma poorly depicted by ^{123}I-MIBG and better depicted by ^{111}In-octreotide. (A) Three overlapping posterior ^{123}I-MIBG scans which demonstrate only one pheochromocytoma deposit in the abdomen (arrow). Note the normal uptake in salivary glands (S), in heart (H), in spleen (SP), in liver (L) and urinary bladder (U). (B and C) Whole body, anterior and posterior ^{111}I-octreotide scans demonstrating multiple pheochromocytoma deposits in the neck, thorax and abdomen (arrows). Note the normal tracer uptake in liver (L), spleen (S), right kidney (K) (the left kidney is absent due to prior surgery) and colon (G). * indicates the only tumoural deposit depicted by both ^{123}I-MIBG and ^{111}In-octreotide.

sensitivity of approximately 65% in detecting metastatic disease especially when spread to the neck and chest (71). ^{111}In-octreotide can be useful in combination with radiocholesterol scintigraphy in patients with corticoadrenal nodular hyperplasia due to an ectopic ACTH hypersecretion. In these cases, radiocholesterol may be used to depict the adrenal disease while ^{111}In-octreotride can be useful to locate the ACTH-producing tumour (14). Lastly, some radiolabelled somatostatin analogues such as ^{90}Y-DOTA-octreotide are used for radioisotope therapy of malignant metastatic neuroendocrine tumours (66).

Adrenal malignancies

A large variety of positron-emitter tracers have been synthesised and are currently under investigation for

adrenal imaging. Some of them are specific for the adrenal cortex (^{11}C-acetate, ^{11}C-etiomidate, ^{11}C-metiomidate) (6) or medulla (^{11}C-hydroxyephedrine, ^{11}C-epinephrine) (47) while others are not tissue specific but are used to detect malignant lesions at all sites including the adrenal, such as ^{11}C-tyrosine, ^{11}C-methionine, ^{11}C-thymidine and ^{18}F-FDG (72). ^{18}F-FDG (FDG) is the most widely used positron-emitter tracer in clinical oncology (72). Deoxy-glucose (DG) is a glucose analogue that enters the cell using specific transmembrane carrier proteins (72). Once within the cytoplasm, DG is phosphorylated to DG-6-phosphate but does not appear to be further metabolised (51). In most malignant tumours there is an increase of glycolytic metabolism which accounts for elevated DG uptake (72). For the purpose of imaging, DG can be radiolabelled with ^{18}F to yield FDG, an efficient PET imaging agent for many tumours. However, an elevated FDG uptake has also been described in acute/ septic and chronic/granulomatous diseases due to the increased glycolytic metabolism of activated leukocytes (73–75).

Patient preparation and FDG-PET technique

An overnight or a 4–6 h fast is required to reduce the circulating pool of glucose (76). In diabetic patients, careful monitoring of blood glucose levels is recommended. If the FDG-PET is performed during, or close to, radio- and/or chemotherapy, there exists a possibility of obtaining false positive or false negative results (77). FDG is injected intravenously at a dosage of 8–20 mCi. Before injection, the patient should be recumbent, relaxed and in a low light and noise environment to prevent physiological increase of FDG uptake in skeletal muscles and some areas of the brain. For imaging, a PET scanner is used to acquire whole body and/or regional images, typically commencing 40–60 min after FDG administration. Attenuation correction is usually applied and quantitative analysis can be performed by calculating the standardised uptake value. Some attempts have been made to obtain FDG imaging using a dual-head gamma camera and the coincidence acquisition method; however, currently, this method shows lower sensitivity and spatial resolution than FDG-PET (78).

Normal FDG biodistribution

FDG normally concentrates in the brain and relatively high tracer uptake is also observed in the kidneys and bladder. Various degrees of uptake can be seen in the heart. Mild uptake is commonly seen in the liver and spleen (72, 76, 77). In some cases, relatively high bowel uptake can interfere with interpretation in the abdomen (72, 77). Finally, a wide range of localisation and intensity can occur in skeletal muscles. This is related to contraction at the time of, or shortly before, FDG administration. In addition to injection in a controlled environment, some investigators administer muscle relaxants and benzodiazepines.

Clinical applications of FDG-PET

FDG is the positron-emitter radiotracer most widely used in clinical practice during the last decade (72). It is currently utilised as a tumour-seeking agent to image both the primary tumour and metastatic disease (e.g. skeletal and visceral metastases) in many types of cancers (72). FDG-PET has been proven to be highly sensitive not only in cancer staging but also during follow-up, to distinguish scar or fibrosis from persistent viable tumours after treatment, for early detection of local relapse or metastases (especially in patients without any clinical evidence of disease but with increased serum tumoural markers), and to monitor the response to therapy (72). The FDG uptake is often related to the degree of malignancy, and tumours that are characterised by rapid growth and aggressive histological grading usually show high FDG uptake (79). In contrast, slow-growing tumours such as many endocrine lesions can show various degrees of FDG uptake (80–82); in particular, some well-differentiated endocrine tumours may not be visualised by FDG-PET (80–82). Some authors have argued that FDG uptake by endocrine tumours is related to the aggressiveness of the neoplasm and that high uptake has to be considered as a poor prognostic factor (81, 82). Unfortunately, FDG is not a tumour-specific tracer, because an abnormally increased FDG uptake has also been documented in some benign diseases such as acute and chronic infections and granulomatous diseases (e.g. mycosis, sarcoidosis, osteomyelitis and others) (72, 74). The elevated FDG uptake in these diseases has been related to increased glycolytic metabolism by activated leukocytes.

As far as the adrenal is concerned, most of the studies reported have dealt with the potential role of FDG-PET in the staging of patients with known extra-adrenal cancers (8, 83, 84). It has been well documented that FDG-PET provides a greater sensitivity than traditional radiologic imaging (8, 72, 80, 82–85). In this regard, patients with lung cancer (the tumour which most frequently spreads to the adrenal) have been extensively studied, and FDG-PET has been proven to reveal additional, unknown metastatic foci in 19–34% of cases (8, 72, 83, 84). Specifically, the prevalence of adrenal metastases discovered by FDG-PET has been reported to be as high as 9.9% in several studies (8, 83, 84). The upstaging resulting from FDG-PET can play an important role in the planning of therapeutic strategies in oncologic patients (e.g. solitary metastasis to the adrenal may be resected together with the primary with curative intent) (Fig. 14) (8, 72, 83, 84). In some patients, the adrenal metastasis can be the first manifestation of a cancer, and FDG-PET has been proven to be useful in locating the primary tumour (86).

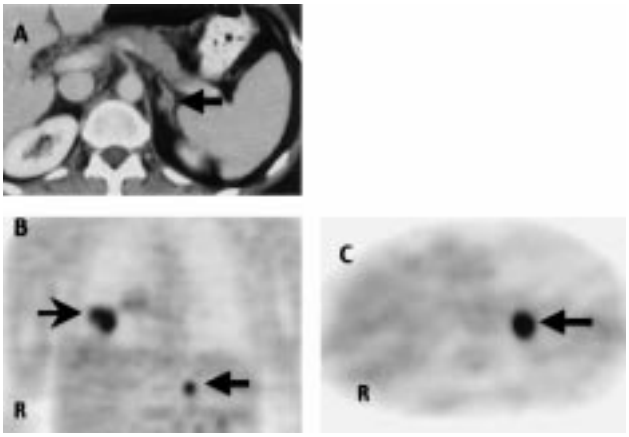

Figure 14 Recurrent non-small cell carcinoma of the right lung depicted by FDG-PET and CT scan with concomitant solitary metastasis to left adrenal gland. A 40-year-old male with a suspected recurrence of a non-small cell carcinoma of the right lung, after right lower lobe resection. (A) Detail of transverse abdominal CT showing enlargement of the left adrenal gland (black arrow). (B) Coronal FDG-PET scan of chest and abdomen demonstrates abnormal focal tracer uptake in recurrent thoracic primary tumour (black arrow) and left adrenal metastasis (black arrow). (C) Tranverse abdominal FDG-PET scan demonstrates intense abnormal focal uptake in left adrenal metastasis (arrow). Note the faint normal liver tracer uptake. R, right (in B) and (C)).

Primary malignancies arising from the adrenal cortex represent a rare condition; in these cases FDG-PET is useful in the localisation of distant metastases (87).

Two other major topics have to be discussed: (a) the utility of FDG-PET in depicting pheochromocytomas and related lesions, and (b) the role of FDG-PET in distinguishing benign from malignant adrenal masses, particularly those discovered incidentally.

Regarding the first topic, Shulkin *et al.* (88) have studied a large group of patients with pheochromocytoma, both benign and malignant, and compared results of MIBG scintigraphy with FDG-PET. The authors found that most malignant pheochromocytomas (14/17; 82%) and, in addition, a considerable percentage of benign pheochromocytomas (7/12 cases; 58%) were depicted by FDG-PET. Moreover, in patients with malignant pheochromocytomas, the FDG-PET was highly sensitive for revealing metastatic spread. However, it has to be emphasised that the sensitivity of MIBG was greater than that of FDG, both in benign (83% versus 58%) and malignant pheochromocytomas (88% versus 82%). Furthermore, in cases positive with both MIBG and FDG, the tumour and its metastases were better depicted with MIBG than with FDG. All pheochromocytomas which failed to concentrate FDG were well depicted by MIBG. Nevertheless, it is interesting to note that in four patients in whom MIBG was negative, the FDG-PET was able to locate the tumour. Thus, there is a complementary role for both MIBG and FDG in pheochromocytoma and, in particular, FDG can be useful as a second-line imaging modality to visualise the small minority of pheochromocytomas that do not accumulate MIBG (88).

Regarding the potential role of FDG-PET in distinguishing benign from malignant adrenal masses, particularly those disclosed by CT, MRI and ultrasound performed for the investigation of non-adrenal diseases (e.g. abdominal pain, staging of various cancers such as lung) so called 'incidentalomas', FDG-PET may have an increasing importance. In a study by Boland *et al.* (8), a series of 24 adrenal masses initially revealed by CT scan in 20 cancer patients were investigated and FDG-PET was able to discriminate adrenal metastases (14/14) from benign adrenal masses (10/10) in all cases with 100% accuracy. Erasmus *et al.* (84) performed FDG-PET in a group of 27 patients with bronchogenic carcinoma and concomitant adrenal mass(es). FDG-PET depicted all the adrenal metastatic lesions ($n = 25$) and was correctly negative in 8/10 benign adrenal masses. However, significant FDG concentration was observed in 2/10 benign adrenal masses (8% false positive rate). Thus, in this study, the FDG-PET showed 100% sensitivity and 80% specificity in detecting adrenal malignancy. Despite the favourable results, it has to be emphasised that these studies were performed in selected groups of oncologic patients, i.e. in patients with an expected prevalence of adrenal metastases considerably greater than in the general population (26, 27). Furthermore, it has been well established that the majority of cases of 'incidentaloma' are discovered in non-oncologic patients in whom the probability of malignancy (either primary or metastatic) is rather low (26, 27). In a recent study by Maurea *et al.* (89), an unselected group of 27 patients with unilateral adrenal incidentaloma depicted at CT or MRI were investigated. Interestingly, 82% of the enrolled patients were studied for reasons other than clinical staging of a known extra-adrenal cancer and 81% of them had a non-hypersecretory adrenal mass. They found that 13/14 (93%) of the benign adrenal masses, including five adrenal adenomas, did not show FDG uptake; the only exception was a case of benign pheochromocytoma which was FDG avid. At the same time, 13/13 (100%) malignant adrenal lesions, including a surprisingly high number of adrenocortical carcinomas ($n = 7$; 53% of all malignant lesions in this series), showed abnormally increased FDG uptake.

Further studies performed on larger numbers of unselected patients with non-hypersecretory adrenal masses are needed to clarify the full potential utility of FDG-PET in distinguishing benign versus malignant adrenal incidentalomas.

Conclusions

By thoughtful exploration of the metabolic characteristics which render the adrenal cortex and medulla and lesions derived from these tissues different from

adjacent structures it has been possible to develop a series of clinically useful radiopharmaceuticals for both diagnosis (including planar scintigraphy, SPECT and PET) and therapy.

These principles which are broadly applicable may be considered when designing radiopharmaceuticals for use with many other tissues and disease processes.

There remain a wide variety of other adrenal tissue characteristics which might yet be explored to produce other clinically useful radiopharmaceuticals.

References

1 Beierwaltes WH, Wieland DM, Yu T, Swanson D & Mosley S. Adrenal imaging agents: rationale, synthesis, formulation and metabolism. *Seminars in Nuclear Medicine* 1978 **8** 5–21.

2 Counsell RE, Renade VV, Blair RJ, Beierwaltes WH & Weinhold PA. Tumor localizing agents. IX. Radioiodinated cholesterol. *Steroids* 1970 **16** 317–328.

3 Kojima M, Maeda M, Ogawa H, Nitta K & Ito T. New adrenal-scanning agent. *Journal of Nuclear Medicine* 1975 **16** 666–668.

4 Sarkar SD, Beierwaltes WH, Ice RD, Basmadjian GP, Hertzel KR, Kennedy WP *et al.* A new and superior adrenal scanning agent, NP-59. *Journal of Nuclear Medicine* 1975 **16** 1038–1042.

5 Beierwaltes WH, Wieland DM, Mosley ST, Swason DP, Sarkar SD, Freitas JE *et al.* Imaging the adrenal glands with radiolabeled inhibitors of enzymes: concise communication. *Journal of Nuclear Medicine* 1978 **19** 200–203.

6 Bergstrom M, Juhlin C, Bonasera TA, Sunding A, Rastad J, Akerstrom G *et al.* PET imaging of adrenal cortical tumors with the 11beta-hydroxylase tracer 11C-metomidate. *Journal of Nuclear Medicine* 2000 **41** 275–282.

7 Hay RV, Flemming RM, Ryan JW, Williams KA, Strak VJ, Lathrop KA *et al.* Nuclear imaging analysis of human low density lipoprotein biodistribution in rabbits and monkeys. *Journal of Nuclear Medicine* 1991 **32** 1239–1245.

8 Boland G, Goldember MA, Lee MJ, Mayo-Smith WW, Dixon J, McNicholas MM *et al.* Indeterminate adrenal mass in patients with cancer: evaluation at PET with 2-F-18-fluoro-2-deoxy-D-glucose. *Radiology* 1995 **194** 131–136.

9 Gross MD, Shapiro B, Thrall JH, Freitas JE & Beierwaltes WH. The scintigraphic imaging of endocrine organs. *Endocrine Reviews* 1984 **5** 221–281.

10 Shapiro B, Britton KE, Hawkins LA & Edwards CE. Clinical experience with 75-Se-selenomethylcholesterol adrenal imaging. *Clinical Endocrinology* 1981 **15** 19–27.

11 Gross MD, Falke THM & Shapiro B. Adrenal glands. In *Endocrine Imaging*, pp 271–349. Eds MD Sandler, JA Patton, MD Gross, B Shapiro & THM Falke. Connecticut: Appleton & Lange, 1992.

12 Lynn MD, Gross MD & Shapiro B. Enterohepatic circulation and distribution of I-131-iodomethyl-19-norcholesterol (NP-59). *Nuclear Medicine Communications* 1986 **7** 625–630.

13 Shapiro B, Fig L, Gross MD & Khafagi F. Radiocholesterol diagnosis of adrenal disease. *Critical Reviews in Clinical Laboratory Sciences* 1989 **27** 265–298.

14 Gross MD & Shapiro B. Radionuclide imaging of the adrenal cortex. *Quarterly Journal of Nuclear Medicine* 1999 **43** 224–232.

15 Shapiro B, Nakajo M, Gross MD, Freitas JE, Copp JE & Beierwaltes WH. Value of bowel preparation in adrenocortical scintigraphy with NP-59. *Journal of Nuclear Medicine* 1983 **24** 732–734.

16 Ishimura J, Kawanaka M & Fukuchi M. Clinical application of SPECT in adrenal imaging with I-131-6β-iodomethyl-19-norcholesterol. *Clinical Nuclear Medicine* 1989 **14** 278–281.

17 Gross MD, Valk TW, Swanson DP, Thrall JH, Grekin RJ & Beierwaltes WH. The role of pharmacologic manipulation in adrenal cortical scintigraphy. *Seminars in Nuclear Medicine* 1981 **9** 128–148.

18 Thrall JH, Freitas JE & Beierwaltes WH. Adrenal scintigraphy. *Seminars in Nuclear Medicine* 1978 **8** 23–41.

19 Gross MD, Shapiro B & Beierwaltes WH. The functional characterization of the adrenal gland by quantitative scintigraphy. *Recent Advances in Nuclear Medicine* 1983 **6** 83–115.

20 Fig L, Ehrman D, Gross MD, Shapiro B, Schteingart D & Glazer G. The localization of abnormal adrenal function in ACTH-independent Cushing's syndrome. *Annals of Internal Medicine* 1988 **109** 547–553.

21 Pasieka JL, Requeda E, Reach JE, Plouin PF & Savoie JC. Adrenal scintigraphy of well-differentiated (functioning) adrenocortical carcinomas: potential surgical pitfalls. *Surgery* 1992 **112** 884–890.

22 Gross MD, Shapiro B, Freitas JE, Meyers L, Francis IR, Thompson NW *et al.* Clinical significance of the solitary functioning adrenal gland. *Journal of Nuclear Medicine* 1991 **32** 1882–1887.

23 Nomura K, Kusakabe K, Maki M, Ito Y, Aiba M & Demura H. Iodomethylnorcholesterol uptake in an aldosteronoma shown by dexamethasone-suppression scintigraphy: relationship to adenoma size and functional activity. *Journal of Clinical Endocrinology and Metabolism* 1990 **71** 825–830.

24 Gross MD & Shapiro B. Adrenocortical scintigraphy. In *Nuclear Medicine in Clinical Diagnosis and Treatment*, edn 2, pp 805–812. Eds IPC Murray & PJ Ell. London: Churchill & Livingstone, 1998.

25 Gross MD, Shapiro B, Swanson DP, Woodbury M, Schteingart DE & Beierwaltes WH. The relationship of 131I-6β-iodomethyl-19-norcholesterol (NP-59) adrenal cortical uptake to indices of androgen secretion in women with hyperandrogenism. *Clinical Nuclear Medicine* 1984 **9** 264–270.

26 Gross MD & Shapiro B. Clinical review 50: clinically silent adrenal masses. *Journal of Clinical Endocrinology and Metabolism* 1993 **77** 885–888.

27 Kloos RT, Gross MD, Francis IR, Korobkin M & Shapiro B. Incidentally discovered adrenal masses. *Endocrine Reviews* 1995 **16** 460–484.

28 Herrera MF, Grant CS, van Heerden JA, Sheedy PF & Ilstrup DM. Incidentally discovered adrenal tumors: an institutional perspective. *Surgery* 1991 **110** 1014–1021.

29 Glazer HS, Weyman PJ, Sagel SS, Levitt RG & McClennan BL. Nonfunctioning adrenal masses: incidental discovery on computed tomography. *American Journal of Roentgenology* 1982 **139** 81–85.

30 Hussain S, Belldegrun A, Seltzer SE, Richie JP, Gittes RF & Abrams HL. Differentiation of malignant from benign adrenal masses: predictive indices on computed tomography. *American Journal of Roentgenology* 1985 **144** 61–65.

31 Russell RP, Masi AT & Richter ED. Adrenal cortical adenomas and hypertension. A clinical pathologic analysis of 690 cases with matched control and a review of the literature. *Medicine* 1972 **51** 211–225.

32 Allard P, Yankaskas BC, Fletcher RH, Parker LA & Halvorsen RA Jr. Sensitivity and specificity of computed tomography for the detection of adrenal metastatic lesions among 91 autopsied lung cancer patients. *Cancer* 1990 **66** 457–462.

33 Abecassis M, McLoughlin MJ, Langer B & Kudlow JE. Adrenal masses: prevalence, significance, and management. *American Journal of Surgery* 1985 **149** 783–788.

34 Siekavizza JL, Bernardino ME & Samaan NA. Suprarenal mass and its differential diagnosis. *Urology* 1981 **18** 625–632.

35 Siren JE, Haapiainen RK, Huikuri KT & Sivula AH. Incidentalomas of the adrenal gland: 36 operated patients and review of literature. *World Journal of Surgery* 1993 **17** 634–639.

36 Khafagi FA, Gross MD, Shapiro B, Glazer GM, Francis I & Thompson NW. Clinical significance of the large adrenal mass. *British Journal of Surgery* 1991 **78** 828–833.

37 Dominguez-Gadea L, Diez L, Bas C & Crespo A. Differential diagnosis of solid adrenal masses using adrenocortical scintigraphy. *Clinical Radiology* 1994 **49** 796–799.

38 Lee MJ, Hahn PF & Papanicolau N. Benign and malignant adrenal masses: CT distinction with attenuation coefficients, size, and observer analysis. *Radiology* 1991 **179** 415–418.

39 Singer AA, Obuchowshi NA, Einstein DM & Paushter DM. Metastasis or adenoma? Computed tomography evaluation in the adrenal mass. *Cleveland Clinical Journal of Medicine* 1994 **61** 200–205.
40 Mitchell DG, Crovello M, Matteucci T, Petersen RO & Miettinen MM. Benign adrenocortical masses: diagnosis with chemical shift MR images. *Radiology* 1992 **185** 345–351.
41 Greene KM, Brantly PN & Thompson WR. Adenocarcinoma metastatic to the adrenal gland simulating myelolipoma: CT evaluation. *Journal of Computed Assisted Tomography* 1985 **9** 820–821.
42 Heaston DK, Handel DB, Ashton PR & Korobkin M. Narrow gauge needle aspiration of solid adrenal masses. *American Journal of Roentgenology* 1982 **138** 1143–1148.
43 Gross MD, Shapiro B, Bouffard JA, Glazer GM, Francis IR, Wilton GP *et al.* Distinguishing benign from malignant adrenal masses. *Annals of Internal Medicine* 1988 **109** 613–618.
44 Gross MD, Wilton GP, Shapiro B, Cho K, Samuels BI, Bouffard JA *et al.* Functional and scintigraphic evaluation of the silent adrenal mass. *Journal of Nuclear Medicine* 1987 **28** 1401–1407.
45 Bravo EL. Evolving concepts in the pathophysiology, diagnosis, localization and treatment of pheochromocytoma. *Endocrine Reviews* 1994 **15** 356–368.
46 Troncone L, Rufini V, Montemaggi P, Danza FM, Lasorella A & Mastrangelo R. The diagnosis and therapeutic utility of the radioiodinated metaiodobenzylguanidine (MIBG). Five years' experience. *European Journal of Nuclear Medicine* 1990 **16** 325–335.
47 Shapiro B, Gross MD & Shulkin B. Radioisotope diagnosis of malignant pheochromocytoma. *Trends in Endocrinology and Metabolism* 2001 **12** 469–475.
48 Shapiro B, Copp JE, Sisson JC, Eyre PL, Wallis J & Beierwaltes WH. 131-iodine-metaiodobenzylguanidine for the location of suspected pheochromocytoma: experience in 400 cases. *Journal of Nuclear Medicine* 1985 **26** 576–585.
49 Gross MD & Shapiro B. Adrenal hypertension. *Seminars in Nuclear Medicine* 1989 **19** 122–143.
50 Hoefnagel CA. Metaiodobenzylguanidine and somatostatin in oncology: role in the management of neural crest tumours. *European Journal of Nuclear Medicine* 1994 **21** 561–581.
51 Khafagi FA, Shapiro B, Fig LM, Mellette S & Sisson JC. Labetalol reduces iodine-131 MIBG uptake by pheochromocytoma and normal tissue. *Journal of Nuclear Medicine* 1989 **30** 481–489.
52 Lindberg S, Fjalling M, Jacobsson L, Jansson S & Tisell LE. Methodology and dosimetry in adrenal medullary imaging with iodine-131 MIBG. *Journal of Nuclear Medicine* 1988 **29** 1638–1643.
53 Chatal JF & Charbonnel B. Comparison of iodobenzylguanidine imaging with computed tomography in locating pheochromocytoma. *Journal of Clinical Endocrinology and Metabolism* 1985 **61** 769–772.
54 Nakajo M, Shapiro B, Copp J, Kalff V, Gross MD, Sisson JN *et al.* The normal and abnormal distribution of the adrenomedullary imaging agent I-131-metaiodobenzylguanidine (I-MIBG) in man: evaluation by scintigraphy. *Journal of Nuclear Medicine* 1983 **24** 672–682.
55 Bomanji J, Flatman WD, Horne T, Fettich J, Britton KE, Ross G *et al.* Quantitation of iodine-123 MIBG uptake by normal adrenal medulla in hypertensive patients. *Journal of Nuclear Medicine* 1987 **28** 319–324.
56 Bomanji J, Bouloux PMG, Levison DA, Flatman WD, Horne T, Britton KE *et al.* Observations on the function of normal adrenomedullary tissue in patients with phaeochromocytomas and other paragangliomas. *European Journal of Nuclear Medicine* 1987 **13** 86–89.
57 Bomanji J, Levison DA, Flatman WD, Horne T, Bouloux PMG, Ross G *et al.* Uptake of iodine-123 MIBG by pheochromocytomas, paragangliomas, and neuroblastomas: a histopathological comparison. *Journal of Nuclear Medicine* 1987 **28** 973–978.
58 Shapiro B & Gross MD. Radioiodinated MIBG for the diagnostic scintigraphy and internal radiotherapy of neuroendocrine tumors. In *I Tumori della Cresta Endocrina*, pp 65–94. Ed. L Troncone. Modena: Arcadia, 1991.
59 Shapiro B, Sisson JC, Lloyd R, Nakajo M, Satterlee W & Beierwaltes WH. Malignant pheochromocytoma: clinical, biochemical and scintigraphic characterization. *Clinical Endocrinology* 1984 **20** 189–203.
60 Kalff V, Shapiro B, Lloyd R, Sisson JE, Holland K, Nakajo M *et al.* The spectrum of pheochromocytoma in hypertensive patients with neurofibromatosis. *Archives in Internal Medicine* 1982 **142** 2092–2098.
61 Troncone L & Rufini V. MIBG in the diagnosis of neural crest tumours. In *Nuclear Medicine in Clinical Diagnosis and Treatment*, edn 2, pp 843–858. Eds IPC Murray & PJ Ell. London: Churchill & Livingstone, 1998.
62 Goodfellow PJ & Wells SA Jr. RET gene and its implications for cancer. *Journal of the National Cancer Institute* 1995 **87** 1515–1523.
63 Guerra UP, Pizzocaro L, Terzi A, Giubbini R, Maira G, Pagliaini R *et al.* New tracers for the imaging of the medullary thyroid carcinoma. *Nuclear Medicine Communications* 1989 **5** 285–295.
64 Casara D, Rubello D, Tamagnini P, Bernante P & Pelizzo MR. 99mTc-MIBI scintigraphy: an effective imaging technique in detecting loco-regional metastases of medullary thyroid carcinoma. *Journal of Nuclear Medicine* 2001 **42** 323 (Abstract).
65 Krenning EP, Kwekkeboom DJ, Reubi JC & Lamberts SWJ. Somatostatin receptor scintigraphy with 111In-DTPA-D-Phe1-octreotide. In *Nuclear Medicine in Clinical Diagnosis and Treatment*, edn 1, pp 757–764. Eds IPC Murray & PJ Ell. London: Churchill & Livingstone, 1994.
66 Krenning EP, Bakker WH, Kooij PPM, Breeman WA, Oei HY, de Joug M *et al.* Somatostatin receptor scintigraphy with 111In-DTPA-D-PHE1-octreotide in man: metabolism, dosimetry and comparison with 123-Try-3-octreotide. *Journal of Nuclear Medicine* 1992 **33** 652–658.
67 Gibril F, Reynolds JC, Doppman JL, Chen CC, Venzond J, Termanini B *et al.* Somatostatin receptor scintigraphy: its sensitivity compared with that of other imaging methods in detecting primary and metastatic gastrinomas. A prospective study. *Annals of Internal Medicine* 1996 **125** 26–34.
68 Van Royen EA, Verhoeff NP, Meylaerts SA & Miedema AR. Indium-111-DTPA-octreotide uptake measured in normal and abnormal pituitary glands. *Journal of Nuclear Medicine* 1996 **37** 1449–1451.
69 Kwekkeboom DJ, Krenning EP, Bakker WH, Oei HY, Kooij PP & Lamberts SW. Somatostatin analogue scintigraphy in carcinoid tumors. *European Journal of Nuclear Medicine* 1993 **20** 283–292.
70 Cadiot G, Lebtahi R, Sarda L, Bonnaud G, Marmuse JN, Kissuzaine C *et al.* Preoperative detection of duodenal gastrinomas and peripancreatic lymph node by somatostatin receptor scintigraphy. *Gastroenterology* 1996 **111** 845–854.
71 Kwekkeboom DJ, Reubi JC, Lamberts SW, Bruining HA, Muldler AH, Oei HY *et al. In vivo* somatostatin receptor imaging in medullary thyroid carcinoma. *Journal of Clinical Endocrinology and Metabolism* 1993 **76** 1413–1417.
72 Strauss LG & Conti PS. The applications of PET in clinical oncology. *Journal of Nuclear Medicine* 1991 **32** 623–648.
73 Wahl RL. Targeting glucose transporters for tumor imaging: sweet idea, sour result. *Journal of Nuclear Medicine* 1996 **37** 1038–1041.
74 Joe A, Hoegerle S & Moser E. Cervical lymph node sarcoidosis as a pitfall in F18 FDG positron emission tomography. *Clinical Nuclear Medicine* 2001 **26** 542–543.
75 Kalicke T, Schmite A, Risse JH, Arens S, Kelelr E, Hausis M *et al.* Fluorine-18 fluorodeoxyglucose PET in infections bone diseases: results of histologically confirmed cases. *European Journal of Nuclear Medicine* 2000 **27** 524–528.
76 Lindholm P, Minn H, Leskinen-Kallio S, Bergman J, Ruotsalainen U & Joensu H. Influence of the blood glucose concentration of FDG uptake in cancer – a PET study. *Journal of Nuclear Medicine* 1993 **34** 1–6.
77 Strauss LG. Fluorine-18 deoxyglucose and false-positive results: a major problem in the diagnosis of oncological patients. *European Journal of Nuclear Medicine* 1996 **23** 1409–1415.

78 Martin WH, Delbeke D, Patton JA & Sandler MP. Detection of malignancies with SPECT versus PET, with 2-fluorine-18-2-deoxy-D-glucose. *Radiology* 1996 **198** 225–231.
79 Lapela M, Leskinen S, Minn HR, Lindholm P, Kleim PJ, Soderstrom KO *et al.* Increased glucose metabolism in untreated non-Hodgkin's lymphoma: a study with positron emission tomography and fluorine-18-fluorodeoxyglucose. *Blood* 1995 **86** 3522–3527.
80 Gasparoni P, Rubello D & Ferlin G. Potential role of fluorine-18-deoxyglucose (FDG) positron emission tomography (PET) in the staging of primitive and recurrent medullary thyroid carcinoma. *Journal of Endocrinological Investigation* 1996 **20** 527–530.
81 Adams S, Baum R, Rink T, Ashunam-Drager PM, Usadel KH & Hor G. Limited value of fluorine-18 fluorodeoxyglucose positron emission tomography for the imaging of neuroendocrine tumours. *European Journal of Nuclear Medicine* 1998 **25** 79–83.
82 Pasquali C, Rubello D, Sperti C, Gasparoni P, Lessi G, Ferlin G *et al.* Neuroendocrine tumor imaging: can 18F-fluorodeoxyglucose positron emission tomography detect tumors with poor prognosis and aggressive behavior? *World Journal of Surgery* 1998 **22** 588–592.
83 MacManus MP, Hicks RJ, Matthews JP, Hogg A, McKenzie AF, Wirth A *et al.* High rate of unsuspected distant metastases by PET in apparent stage III non-small-cell cancer: implication for radical radiation therapy. *International Journal of Radiation Oncology and Biological Physiology* 2001 **50** 287–293.
84 Erasmus JJ, Patz EF Jr, McAdams HP, Murray JG, Herndon J, Coleman RE *et al.* Evaluation of adrenal masses in patients with bronchogenic carcinoma using 18F-fluorodeoxyglucose positron emission tomography. *American Journal of Roentgenology* 1997 **168** 1357–1360.
85 Casara D & Rubello D. Diagnostic scintigraphy in postoperative staging and follow-up of differentiated thyroid carcinoma. *Rays* 2000 **25** 207–219.
86 Trampal C, Sorensen J, Engler H & Langstrom B. 18F-FDG whole body positron emission tomography (PET) in the detection of unknown primary tumors. *Clinical Positron Imaging* 2000 **3** 160–164.
87 Schumacher T, Brink I, Morer E & Nietzsche EU. Imaging of an adrenal cortex carcinoma and its metastasis with FDG-PET. *Nuklearmedizin* 1999 **38** 124–126.
88 Shulkin BL, Thompson NW, Shapiro B, Francis IR & Sisson JC. Pheochromocytomas: imaging with 2-fluorine-18-fluoro-2-deoxy-D-glucose PET. *Radiology* 1999 **212** 35–41.
89 Maurea S, Mainolfi C, Bazzicalupo L, Panico MR, Imparato C, Alfano B *et al.* Imaging of adrenal tumors using FDG PET: comparison of benign and malignant lesions. *American Journal of Roentgenology* 1999 **173** 25–29.

Received 17 October 2001
Accepted 20 March 2002